Journal of Electrical Engineering 7 (2019) 28-38
doi: 10.17265/2328-2223/2019.01.006

Research and Design of Inverter Applied in Solar PV Systems Connected to Distribution Grid

Nguyen Duc Minh[1], Trinh Trong Chuong[2], Bui Van Huy[2], Quach Duc Cuong[2] and Bui Dinh Thanh[3]

1. Institute of Energy Science, Vietnam Academy of Science and Technology, 18 Hoang Quoc Viet street, Cau Giay district, Hanoi 10072, Vietnam

2. Hanoi University of Industry, No. 298, Cau Dien street, Bac Tu Liem district, Hanoi 11915, Vietnam

3. Hanoi University of Mining and Geology, No.18, Pho Vien, Duc Thang ward, Bac Tu Liem district, Hanoi 11910, Vietnam

Abstract: This paper presents the results of research on the application of inverter in the grid connected solar photovoltaics (PV) system. The main content of the article is to control the three-phase grid connected inverter to meet the requirement of controlling the reactive power to zero at a node of the distribution network while maximizing the active power transmitted to the grid. The control circuits are synthesized on the dq coordinate system and verified on the simulation model by Matlab/Simulink. Both simulation and experimental prototype on 5 kW inverter, being connected to low voltage grid, have been built to show the good results and the practical readiness for implementation.

Key words: SVPWM, reactive power, solar PV, grid connected inverter.

Symbol

Symbol	Unit	Definition
Q	VAr	Measuring and calculation value of reactive power
P	W	Measuring and calculation value of active power
L	H	Inductor
C	F	Capacitor
e_N	V	Alternating power voltage
e_d, e_q	V	Grid voltage on dq coordinates
i_L	A	Current through the coil
i_d, i_q	A	Current through the coil on dq coordinates

1. Introduction

In grid connected solar power systems, the inverter plays an importance role in control systems, as the generated power of solar photovoltaics (PV) system constantly alters due to the weather condition. The alternation of generated power can cause negative impacts on power quality of the grid, such as voltage fluctuation, change in power factor, frequency fluctuation, the increase in the harmonic distortion, etc. The higher and higher demand on the power quality has set out a practical requirement about the necessity of having inverters that can connect flexibly, exchange power and ensure the power quality standards. The aim of the inverter is controlling power among the grid sectors to obtain the most productive capacity of the generator while avoiding sudden conflicts due to loss of transmission or the instability of the generator itself [1]. Apart from the inverter structure, the precision control and stability of electric loop circuit are primary factors in a successful power exchange process.

The main content of this research is to set up control sequences to ensure the control of power factor by 1 and maximize the active power from the solar PV generator to the grid (applied to the non-battery grid connected system). The algorithm and control sequences are systematically analyzed, the research results are proven with the simulated diagram on Matlab and Simulink. They are then verified by a 5 kw experimental model with a PV input that is replaced by a DC source.

Corresponding author: Nguyen Duc Minh, MSc, research fields: electrical system and automatics.

2. Structure of the System and the Controlling Circuit

Fig. 1 presents the diagram of the grid connected solar PV system without backup battery. In this system, DC/DC sets are responsible for executing the power tracking algorithm by the maximum power point tracking (MPPT) algorithm. The DC/AC set must generate a sine-pattern output voltage, ensuring the system's connection (synchronization and monitoring of grids) [2]. The inverter also performs the exchange functions of active power and reactive power between solar PV system and the grid.

2.1 DC/DC Converter

The selected DC/DC converter in the solar PV system is a set of Boost Converter (also known as direct current booster) that is structured as Fig. 2. The controller of the Boost Converter has input voltage given from the solar PV system U_{PV} (Fig. 3). The output of the controller is U_{DC} which processes input for the DC/AC inverter. The MPPT algorithm is involved in this voltage conversion. In this study, the research team used the P&O (Perturb and Observer) MPPT algorithm [3]. This method is simple, popular and easy-to-perform [4].

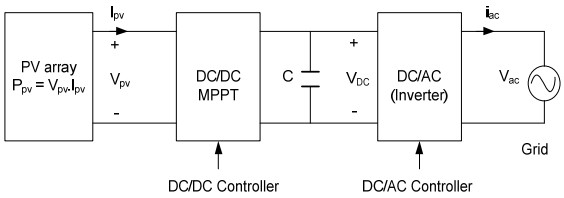

Fig. 1 Principle of grid-connected solar system without battery.

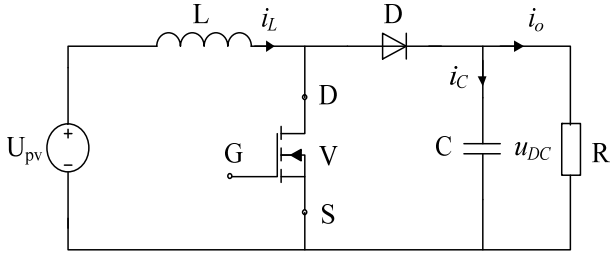

Fig. 2 DC-DC Boost Converter.

This algorithm considers the increase and decrease in voltage periodically to find out the most productive working point. If the variation of voltage makes the power increase, the next variation will remain in the trend of increase or decrease [5]. Conversely, if the variation makes the power decrease, the next variation will change in contrast. When the largest capacity of the working point is defined on the characteristic curve, the voltage variation will fluctuate around the MPPT point (Fig. 4) [6].

The voltage fluctuation causes power loss in the solar PV system [7], especially when the weather conditions change slowly or are stable. This problem can be solved by adjusting logics in P&O algorithm presented in Fig. 5. The P&O algorithm well functions when the weather conditions change dramatically, the maximum power point tracking reaction in a short time and minor adjustments.

The MPPT controller will measure the value of current I and voltage V, then calculate the deviation ΔP, ΔV and check:

- If $\Delta P \cdot \Delta V > 0$, increasing the reference voltage value V_{ref}.
- If $\Delta P \cdot \Delta V < 0$, reducing the reference voltage value V_{ref}.

then replace the previous values with the new V, P value and measure the parameters I, V for the next working cycle. Overall structure of the DC/DC controller system is displayed in Fig. 6.

2.2 DC/AC Inverter

The DC/AC inverter in Fig. 1 is a 3-phase, grid connected inverter. Its circuit structure is presented in Fig. 8, and its function is to convert DC into an AC of 50-60 Hz frequency. When the inverter is applied in a grid connected system, the shortened circuit (one line diagram) of the inverter as Fig. 6 includes converter, R_FC_F filter to minimize the impact of beat rate of current on the voltage frequency of the grid. The inductor L with L_D inductive and R_D resistance is used to balance the voltage difference between the grid and

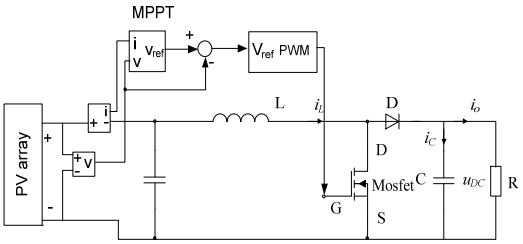

Fig. 3 Principle diagram of Boost Converter controller with MPPT [9].

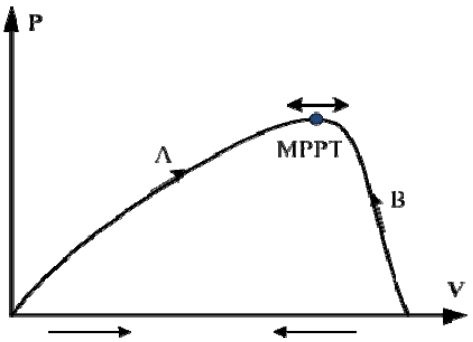

Fig. 4 P&O method to find the largest working power point.

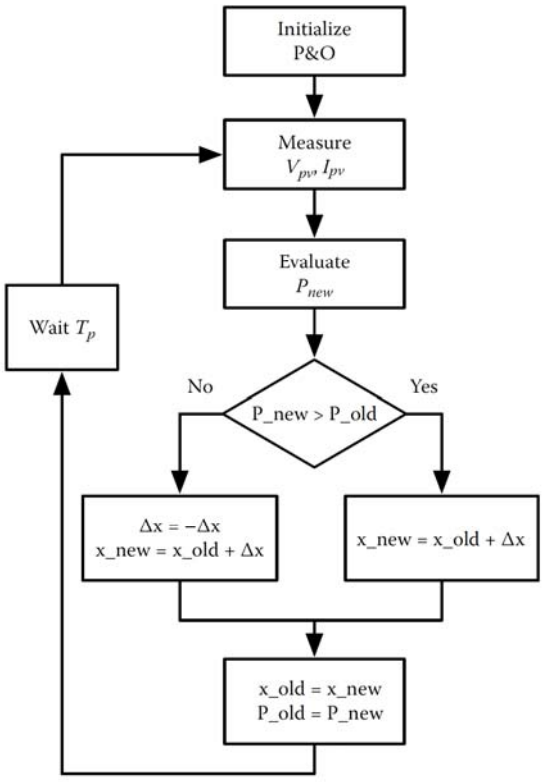

Fig. 5 Steps of conducting P&O method.

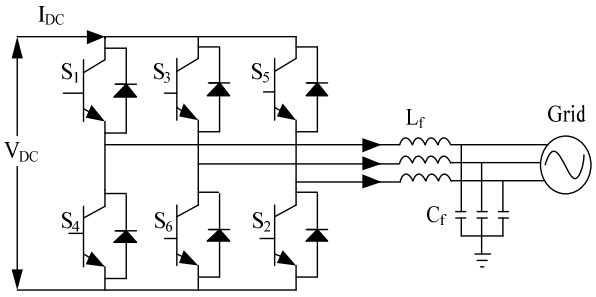

Fig. 6 Structure of three-phase grid-connected inverter.

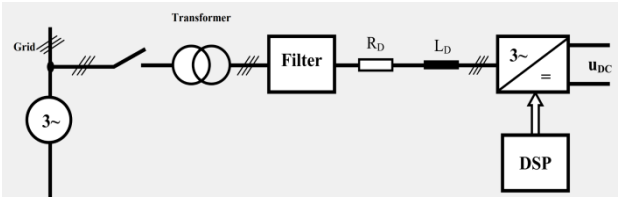

Fig. 7 Principle diagram of grid [8].

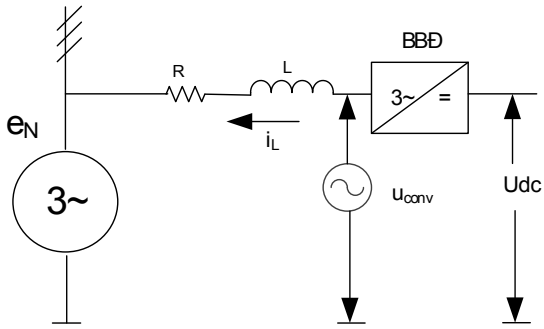

Fig. 8 Alternative diagram of grid circuit.

the output of the converter and to "smooth" the electric current, transformer and circuit breaker. In this study, products with capacity of 5 kW are not too large, so it is possible to omit the capacitors. The principle diagram of the grid connected converter without these steps is shown in Fig. 7.

The circuit including the converter, to filter the chopping impulse voltage, an RC filter, and the inductor L with L_D inductive and R_D resistance are used to filter the current and balance the voltage differences between the grid and the output of the converter, electric current, transformer and circuit breaker. However, it is a system without transformer and filter process. The structure of the grid connected converter is presented as Fig. 8.

When energy transmitted to the grid, the converter functions as an inverter which generates energy from the current circuit to the grid [9]. When the energy transmitted from the grid to the converter, the converter functions as a rectifier, charging energy into the intermediate DC circuit [10]. Applied Kirchhoff law on the alternative diagram:

$$u = Ri_L + L\frac{di}{dt} + e_N \tag{1}$$

Rewrite Eq. (1) on dq coordinates:

$$\begin{cases} \dfrac{di_{Ld}}{dt} = -\dfrac{R}{L}i_{Ld} + \omega i_{Lq} + \dfrac{1}{L}\left(u_d - e_{Nd}\right) \\ \dfrac{di_{Lq}}{dt} = -\dfrac{R}{L}i_{Lq} - \omega i_{Ld} + \dfrac{1}{L}\left(u_q - e_{Nq}\right) \end{cases} \tag{2}$$

Eq. (2) is the status model of the grid inverter system. According to Eq. (2) the controlling unit is the voltage output of the grid inverter, the state vector includes two components i_{Ld}, i_{Lq}.

2.3 Construction of Loop Circuit to Control DC/AC

In terms of control, the two-loop structure consists of an inner loop and an outer loop circuit. The inner loop circuit is the current loop circuit. The outer loop is a power or voltage loop circuit with outstanding advantages. The current loop circuit will help the system to control the current, better respond to the load disturbance, turn off the resonance vibration and protect the overcurrent fault [11]. When the circuit is well designed, the design of the outer loop circuit (voltage, power) also becomes easier. For the external controlled circuit, the goal is to be stable, while in the inner circuit, the requirement is the quick dynamic response capability. Therefore, the authors of the paper proposed a solution of designing a system to control the structure of the two loop circuits as shown in Fig. 9.

2.3.1 Synthesis of Loop Circuit

From Eq. (2), it can be seen that in the loop current equation, there is an interleaving effect between the two axis d and q, and the participation of two grid voltages, called e_d and e_q. The PI controller has the same structure as Eq. (3) to ensure the ability to compensate the channel between the two current components d and q, while also negating the effects of e_d and e_q by the compensatory method:

$$\begin{cases} u_{dref} = \left(K_{p,d} + K_{i,d}\dfrac{1}{s}\right)\Delta I_d + e_d + \omega L i_{Ld} \\ u_{qref} = \left(K_{p,q} + K_{i,q}\dfrac{1}{s}\right)\Delta I_q + e_q + \omega L i_{Ld} \end{cases} \tag{3}$$

in which u_{dref}, u_{qref} are the quantity of output voltage of inverters. The factors of $K_{\text{p,d}}$, $K_{\text{p,q}}$, $K_{\text{i,d}}$, $K_{\text{i,q}}$ are the ratio factors and integral of corresponding adjustment set of axis d and q.

The structure of the inverter controller is shown in Fig. 10. However, due to the current control structure, we have simultaneously offset the channel separation of two components e_d and e_q, in other words the two components e_d and e_q are considered to be disturbance and have been reduced according to the compensatory method; therefore, the obtained system model will consist of two small models on the coordinate axes d, q independently. Ignoring delay due to signal processing delay and sample extracting, the current control structure is shown in Fig. 11.

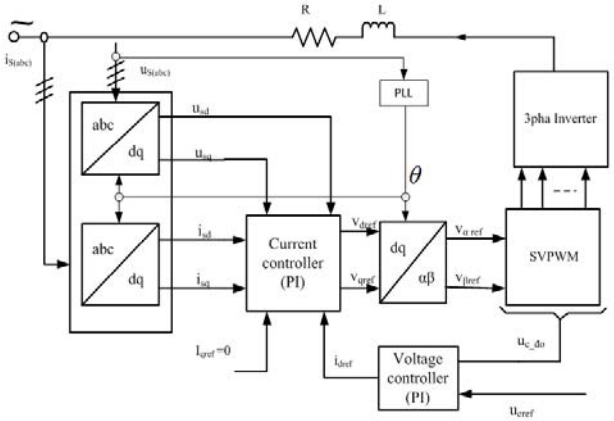

Fig. 9 Structure of grid-connected solar PV controller.

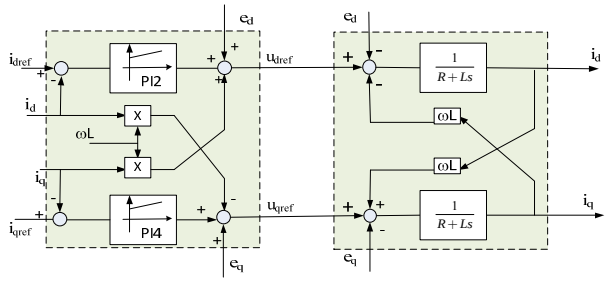

Fig. 10 Structure of controller on dq coordinates.

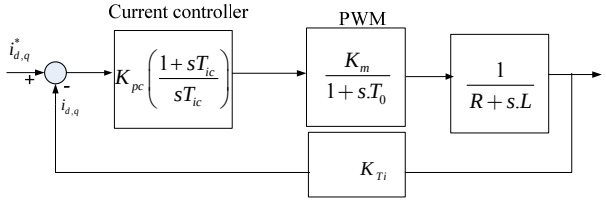

Fig. 11 Block diagram of current controller on dq coordinates.

in which: T_0 is the delay time of the inverter; K_m is the amplification factor of the inverter; K_{Ti} is the measuring factor of the power current; K_{pc}, T_{ic} are factors of the controller according to PI law

Transferring function of the open circuit is presented follows:

$$K_{Go} = K_{pc}\left(\frac{1+sT_{ic}}{sT_{ic}}\right)\frac{1}{1+sT_0}\frac{K_0}{1+sT_L} \quad (4)$$

Synthesize the controller according to the optimization method by quantity [4], the factors of the controller are presented in Eq. (5):

$$T_{ic} = T_L = \frac{L}{R};\ \ Kpc = \frac{T_L}{2K_0.T_0} \quad (5)$$

in which:

$$K_0 = K_m.K_L.K_{Ti}; K_L = \frac{1}{R}; T_L = \frac{L}{R}\ .$$

Replacing into Eq. (4), the transferring function of the open circuit K_{G0} and that of the close circuit are presented in Eq. (6).

$$KG_0 = \frac{1}{2(1+sT_0)};$$
$$K_{Gc}(s) = \frac{I_q(s)}{I_{qref}(s)} = \frac{I_d(s)}{I_{dref}(s)} = \frac{1}{1+s2T_0} \quad (6)$$

$T_{eq} = 2T_0$ is the corresponding time constant of the power controlling circuit. It is prioritized by the quantity.

2.3.2 Construction of DC Voltage Controller

The stage of DC power is the intermediate for exchanging energy between power grid and solar PV system. Controlling of DC voltage on the capacitor means controlling the process of active power exchange. The mission of the intermediate DC voltage controller is to stabilize the total DC voltage value on capacitors, outputs of voltage converter are setting value of the current on axis d. Consequently, in order to control the intermediate DC voltage at gate 1, we have to determine the transferring function between the current on axis d and the intermediate DC voltage value U_{dc}. The active power balance equation of DC and AC is presented in Eq. (7).

$$P = \frac{3}{2}\left(e_d i_d + e_q i_q\right) = u_{dc} i_{dc} - P_{loss} = u_{dc} C\frac{du_{dc}}{dt} - P_{loss} \quad (7)$$

in which: u_C, i_C, P_{loss} is voltage of capacitor, current through the capacitor and power loss of the voltage inverter.

If we ignore the power loss of the voltage inverter and consider the AC power to be symmetric, we have $e_q = 0$, e_d is the amplitude of phase power [10], Eq. (7) will become Eq. (8). Therefore, we have the close loop diagram of the DC voltage converter as in Fig. 12.

$$\frac{du_{dc}}{dt} = \frac{3e_d i_d}{2u_{dc}}\frac{1}{C} \quad (8)$$

In Fig. 13, T_{eq} is the delay time of the current loop circuit; T_f is the delay time of the intermediate DC voltage measuring process on capacitors, K_{Ti} is the current measuring factor. We can simplify the diagram with hypothesis that $T_{\Sigma 2} = T_{eq} + T_f$.

Applying the symmetric priority standard, we can identify the parameters of PI controller as in Eq. (10), with a being the optional parameter.

$$T_{iu} = aT_{\Sigma 2};\ K_{pu} = \frac{2K_{Ti}CU^*_{dc}}{3e_d T_{\Sigma 2}\sqrt{a}} \quad (9)$$

According to Refs. [1, 6, 8]: in order to control Q, we need to control current I_q. In case of grid-connected PV, in order to obtain the highest power

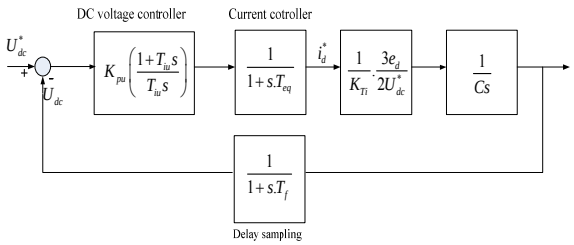

Fig. 12 Block diagram of intermediate DC voltage controller loop.

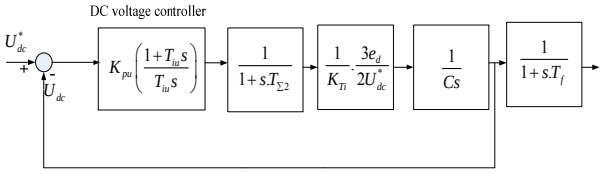

Fig. 13 Equivalent diagram of intermediate DC voltage controller loop.

factor, we select the setting value $i_{qref} = 0$, thereafter, according to Ref. [1], reactive power of the inverter will be 0.

2.4 Principle to Modulate the Space Vector for Inverter (SVPWM)

As presented in Fig. 14, output of loop circuit controlling the current, requires the converting stages of the coordinate from dq/αβ to put into the stage of space vector modulation (SVPWM). The algorithm to modulate the space vector for the 3-phase inverter is presented in Refs. [2, 5]. SVPWM is completely digitalized. The algorithm is simple, easy to apply on the microchips. The algorithm of space vector modulation needs to ensure the output voltage VSI being corresponding to the desired input. The setting value is the desired output voltage, which can be presented in form of polar coordinates $u = U_0.e^{j\theta}$, or perpendicular coordinates u = (u_α, u_β) as in Fig. 15. Vectors $u_{0,1,2,3,4,5,6,7}$ are standard vector, corresponding to the open and close status of valves.

Followings are steps to apply the algorithm to modulate the space vector [2]:

Step 1: Identify the sector of output vector, among 6 sectors presented in Fig. 14. This can be applied in Table 1 and algorithm flowchart in Fig. 15 with $u_\beta^* = u_\beta/\sqrt{3}$.

Step 2: The voltage vector will be synthesized from 2 standard vectors in each sector, therefore, we need to determine the time for executing these 2 standard vectors in the modulation cycle; the inverting circuit status will be zero vector for the remaining time. Fig. 14 presents the voltage vector which is synthesized from 2 standard vectors of u_1 and u_2. The algebraic method is used to determine the modulation factor for voltage vector from two most updated standard vectors in each sector (the modulation factor is the ratio between execution time of standard vectors in each modulation cycle).

As the length of status vector is standardized, with $U_i = (2/3)U_{DC}$, the vectors are presented in the following cordinate, take $\mathbf{u_1}$, $\mathbf{u_2}$ as examples:

$$\mathbf{u_1} = U_i[1,0]; \mathbf{u_2} = U_i\left[\frac{1}{2}, \frac{\sqrt{3}}{2}\right] \quad (10)$$

The systhesis of vector **u** through $\mathbf{u_1}$, $\mathbf{u_2}$ gives out the following equation:

$$\mathbf{u} = d_1\mathbf{u}_n + d_2\mathbf{u}_m \quad (11)$$

$\mathbf{u}_n, \mathbf{u}_m$ are two standard vectors in each sector. Factors of d_1, d_2 are calculated according to Eq. (11) and Table 2. For the remaining time, the zero vector will be executed, with the modulation factor of $d_0 = 1 - d_1 - d_2$.

Step 3: The next step is from the modulation factor to execute the standard vectors, it is necessary to determine the modulation factor for each semiconducting valve of the inverter circuit. In order to determine the modulation factor of each semiconducting valve, it is necessary to construct the pulse sample for each sector. This pulse sample is introduced in order to ensure the smallest number of switching of the semiconductor valves in inverter circuit.

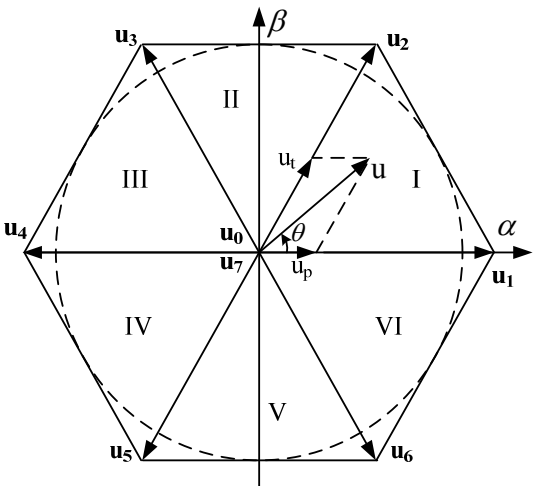

Fig. 14 Space vector, status vectors and sectors.

Table 1 Inequation to determine the position of *u* in sector [2].

$u_\beta \geq 0$	Sector I	Sector II	Sector III
	$u_\beta \geq 0$ $u_\beta < \sqrt{3}u_\alpha$	$u_\beta \geq \sqrt{3}u_\alpha$ $u_\beta > -\sqrt{3}u_\alpha$	$u_\beta \geq 0$ $u_\beta < -\sqrt{3}u_\alpha$
$u_\beta < 0$	Sector IV	Sector V	Sector VI
	$u_\beta < 0$ $u_\beta \geq \sqrt{3}u_\alpha$	$u_\beta < \sqrt{3}u_\alpha$ $u_\beta \leq -\sqrt{3}u_\alpha$	$u_\beta < 0$ $u_\beta \geq -\sqrt{3}u_\alpha$

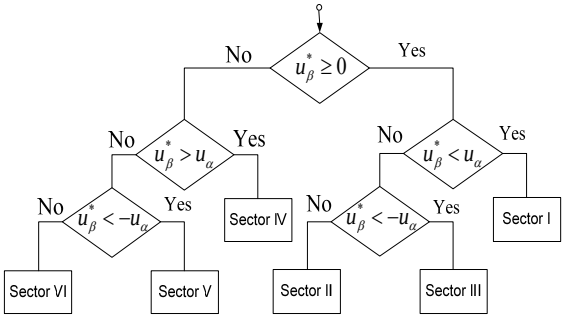

Fig. 15 Algorithm diagram to determine sectors.

Table 2 Matrix synthesis in each sector.

Sector 1 $\mathbf{A}_{nm} = \frac{1}{U_{dc}}\begin{pmatrix} \frac{3}{2} & -\frac{\sqrt{3}}{2} \\ 0 & \sqrt{3} \end{pmatrix}$	Sector 2 $\mathbf{A}_{nm} = \frac{1}{U_{dc}}\begin{pmatrix} -\frac{3}{2} & \frac{\sqrt{3}}{2} \\ \frac{3}{2} & \frac{\sqrt{3}}{2} \end{pmatrix}$
Sector 3 $\mathbf{A}_{nm} = \frac{1}{U_{dc}}\begin{pmatrix} 0 & \sqrt{3} \\ -\frac{3}{2} & -\frac{\sqrt{3}}{2} \end{pmatrix}$	Sector 4 $\mathbf{A}_{nm} = \frac{1}{U_{dc}}\begin{pmatrix} 0 & -\sqrt{3} \\ -\frac{3}{2} & \frac{\sqrt{3}}{2} \end{pmatrix}$
Sector 5 $\mathbf{A}_{nm} = \frac{1}{U_{dc}}\begin{pmatrix} -\frac{3}{2} & -\frac{\sqrt{3}}{2} \\ \frac{3}{2} & -\frac{\sqrt{3}}{2} \end{pmatrix}$	Sector 6 $\mathbf{A}_{nm} = \frac{1}{U_{dc}}\begin{pmatrix} \frac{3}{2} & \frac{\sqrt{3}}{2} \\ 0 & -\sqrt{3} \end{pmatrix}$

$$\begin{bmatrix} d_1 \\ d_2 \end{bmatrix} = \frac{1}{U_{dc}}\begin{pmatrix} \frac{2}{3} & \frac{1}{3} \\ 0 & \frac{1}{\sqrt{3}} \end{pmatrix}^{-1}\begin{bmatrix} u_{S\alpha} \\ u_{S\beta} \end{bmatrix} = \frac{1}{U_{dc}}\begin{pmatrix} \frac{3}{2} & -\frac{\sqrt{3}}{2} \\ 0 & \sqrt{3} \end{pmatrix}\begin{bmatrix} u_{S\alpha} \\ u_{S\beta} \end{bmatrix} = \mathbf{A}_{nm}\begin{bmatrix} u_{S\alpha} \\ u_{S\beta} \end{bmatrix} \quad (12)$$

3. Modelling and Experiment

3.1 System Modelling

The simulation diagram of the controlling system of the inverter using Matlab/Simulink software is presented in Fig. 16, in which the VSC Control is the stage of executing the controlling algorithm of the 3-phase voltage inverter. The configuration of the controller is presented in Table 3 [11].

Boost Converter, or so-called DC-DC voltage converter, gives out the output voltage which is larger than the input voltage (simulation diagram in Fig. 17). The basic circuit contains 2 switching semiconductors (one diode and one transistor) and a coil L, a capacitor C, load R. The MPPT controller uses the algorithm with maximum capacity P&O as presented above.

The analysis results of the model, presented in Fig. 18, show that when the solar radiation is about 1,050 (W/m^2), the power *P* generated to the grid is 5 kW. The output voltage of the DC/DC converter is the setting value of the intermediate DC voltage controller U_{DC}. The simulation results of Fig. 19 show that the intermediate DC voltage is stable when the system is at identified status, which means the power exchange process is balanced.

The power quality generated to the grid is good, with the analysis results of current pattern and 4-phase harmonization wave at two presentative points of time t = 2 s as presented in Fig. 20. The simulation results

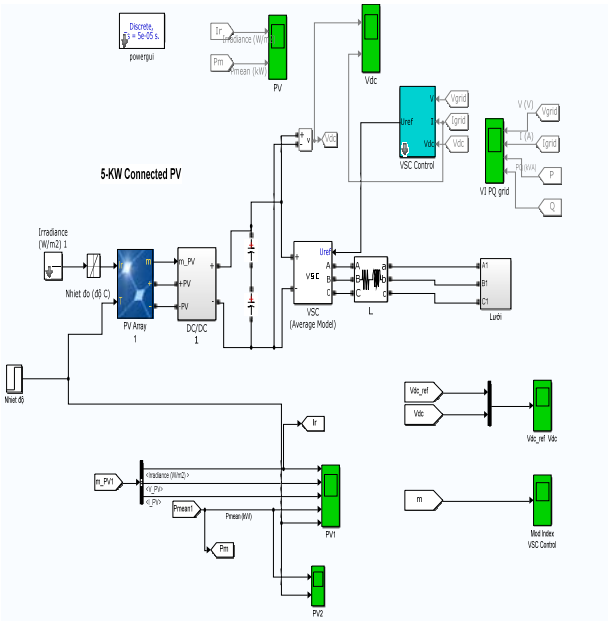

Fig. 16 Simulation diagram of grid-connected solar PV system.

Table 3 Configuration of the controller.

Controller	K_p	K_i
DC voltage controller	20	100
Current controller (dq)	0.015	1

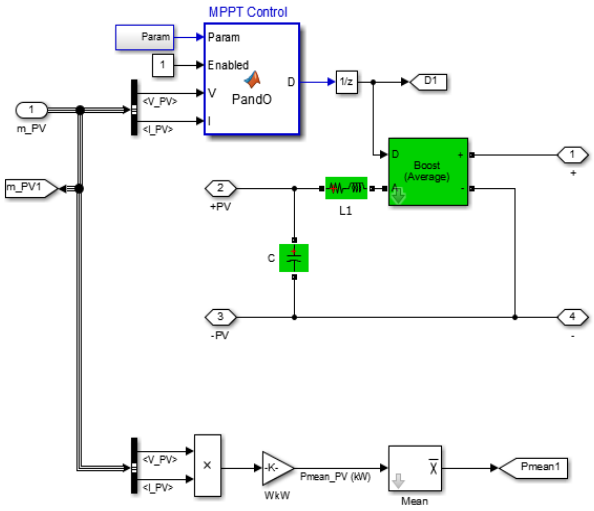

Fig. 17 Explanation diagram of DC/DC.

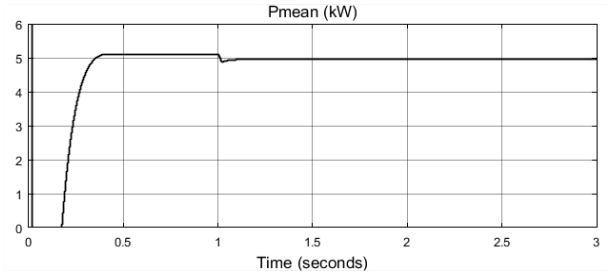

Fig. 18 Active power from PMT to converter.

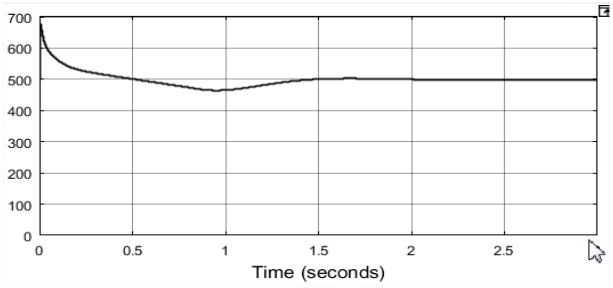

Fig. 19 DC power on capacitor.

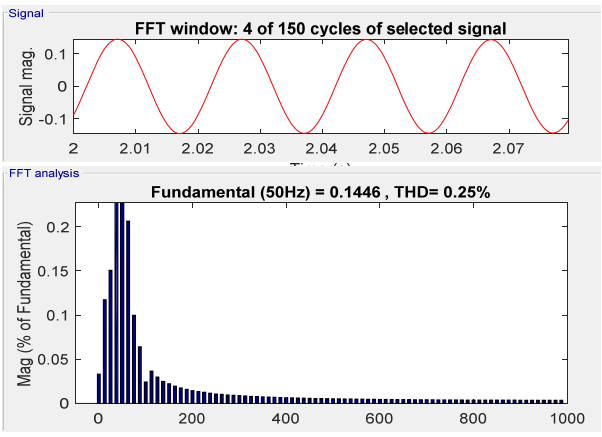

Fig. 20 Analysis of harmonization wave in form of power into the grid at t = 2 s.

of power P, Q in Fig. 21 show that power Q is controlled to 0 in very short time, at around 0.7 s, which ensures the power factor of the current generated to the grid is the highest. The active power generated to the grid is nearly 4.5 kW, compared to the capacity of solar battery generated to the inverter which is 5 kW. The efficiency is about 90%.

3.2 Experiment Results

In order to verify the space vector modulation algorithm for grid-connected three-phase set, we constructed the experimental system. The comprehensive system is presented in Fig. 22. Component modules of the system have been designed and manufactured successfully, as presented in Figs. 23-25. The analysis results of measuring wave patterns into IGBT valves, intermediate DC voltage and analysis results of the harmonization wave are presented in Figs. 26-28.

3.2.1 Efficiency Experiment

We conduct 3 experiment with different loads.

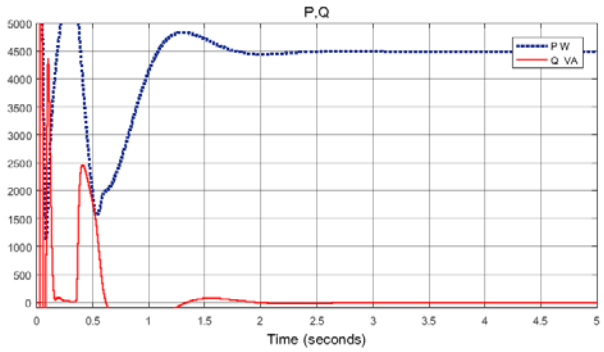

Fig. 21 Active power (dot line) and reactive power (solid line) into the grid.

Fig. 22 Comprehensive equipment.

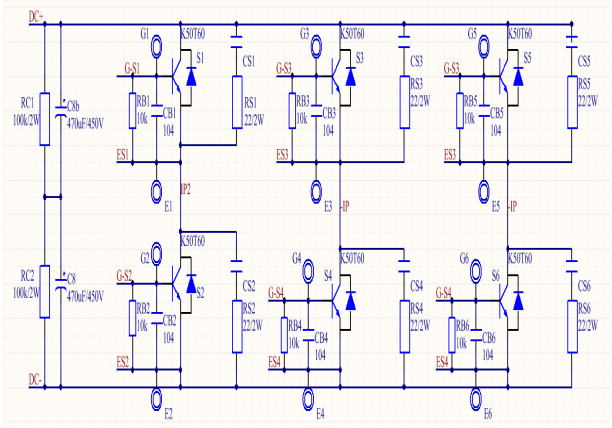

Fig. 23 Diagram of three-phase inverter force circuit.

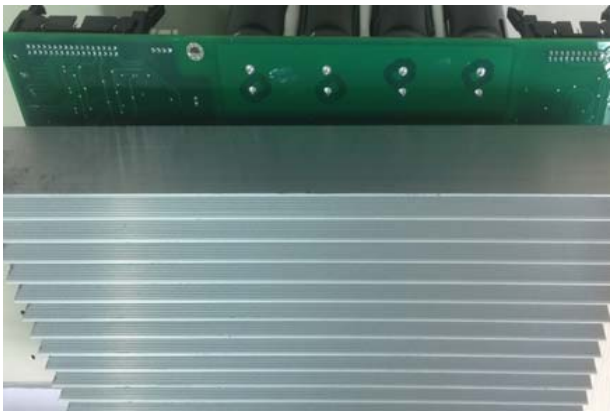

Fig. 24 Block of force circuit with heat radiator.

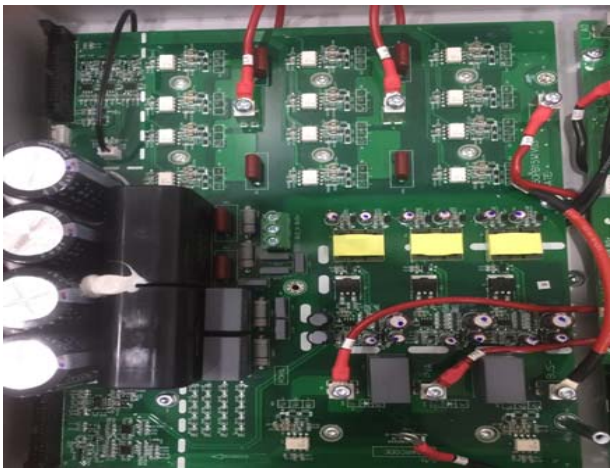

Fig. 25 DC capacitor module and connected block.

1st time: 25 florescent light bulbs 60 W + 8 fans 72 W

- DC input voltage: U_{DCt} = 220 V
- DC input current: I_{iDC} = 9.4 A
- AC output power: P_{AC} = 1,822.33 W

Converting efficiency (%): P_{AC}/P_{DC} = 1,822.33 / (220 × 9.4) × 100% = 88.12%

2nd time: 3 air conditioning systems 9,000 BTU (equivalent to 2,238 kW)

- DC input voltage: U_{DCt} = 220 V
- DC input current: I_{iDC} = 10.17 A
- AC output power: P_{AC} = 2,001.1 W

Converting efficiency (%) P_{AC}/P_{DC} = 2,001.1 / (220 × 10.17) × 100% = 89.43%

3rd time: 3 air conditioning systems 12,000 BTU (equivalent to 2,984 kW)

- DC input voltage: U_{DCt} = 220 V
- DC input current: I_{iDC} = 13.6 A
- AC output power: P_{AC} = 2,690.4 W

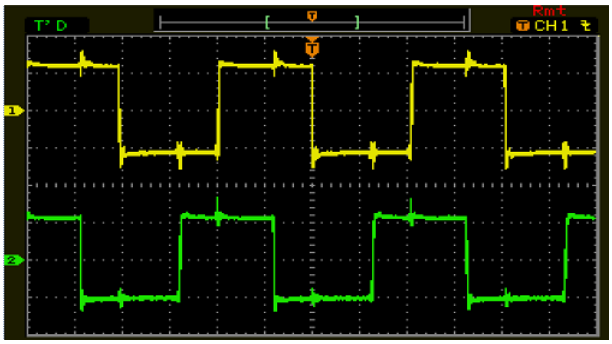

Fig. 26 Measuring wave pattern into the IGBT valve DC-DC and DC-AC modules.

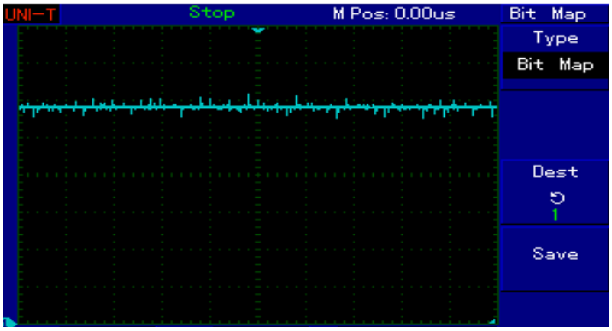

Fig. 27 Intermediate DC power pattern.

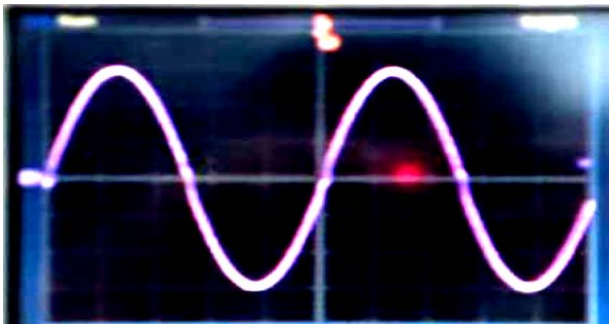

Fig. 28 One-phase power pattern to the grid.

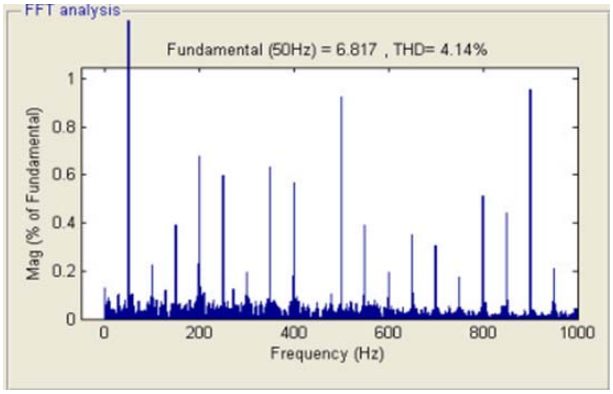

Fig. 29 Analysis results of harmonization wave.

Converting efficiency (%) P_{AC}/P_{DC} = 2,690.4 / (220 × 13.1) × 100% = 89.9%.

Conclusion on converting efficiency after three times of measuring, the average result is 89.15%.

3.2.2 Testing on Harmonization Waves

In line with efficiency evaluation we also measure the harmonization wave spectrum using digital oscilloscope as presented in Fig. 29, the results show that the harmonic distortion is 4.14% (< 5%).

In addition, we also conduct with pure resistant load and inductive load with different capacities, the results show that:

• Output frequency f = 50 Hz with error of ± 0.1 Hz. AC output voltage with effective value meets the requirement, the sin output wave pattern with harmonization component is acceptable.

• The output power meets the requirement of design, when being tested on different loads. The average converting efficiency is 89.15%.

• The DC input voltage from the working solar panel ranges from 16 V to 36 V, which can be expanded to 45 V_{DC}.

4. Conclusion

The article has built a control system for the converter. The DC current and intermediate voltage control loops are analyzed and designed. The paper builds simulation models of input voltage inverter with full physical and systematic significance, based on sufficient assumptions.

Simulation results show that the inverters used in grid-connected solar systems have worked well. The results are convincing and practical. The experimental results on the actual model show good results, proving the proposed solution.

Equipment efficiency will be improved in the near future by raising the hash frequency and selecting highly efficient accessories.

Acknowledgements

This paper is developed as a component of the study "Research, Design and Manufacture of Highly Efficient Inverter Connected to Distribution Grid for Solar PV System" Code: VAST07.04/18-19. The authors specially thank the Vietnam Academy of Science and Technology, Institute of Energy Science for providing fund for the study.

References

[1] Sanchez, C. A. 2010. "Control Design for Electronic Power Converters." Ph.D. thesis, Institut National Polytechnique de Grenoble; Universidad de Sevilla.

[2] Erickson, R. W., and Maksimovic, D. 2001. *Fundamentals of Power Electronics*. New York: Kluwer.

[3] Freeman, D. 2010. *Introduction to Photovoltaic Systems Maximum Power Point Tracking*. Texas Intruments, Application report.

[4] Hwang, J. W. G., Winkelnkemper, M., and Lehn, P. W. 2006. "Design of an Optimal Stationary Frame Controller for Grid Connected AC-DC Converters. IEEE Industrial Electronics." Presented at the IECON 2006- 32nd Annual Conference on IEEE Industrial Electronics, Paris, France.

[5] Quang, N. P., and Dittrich, J. 2008. *Vector Control of Three-Phase AC Machine: System Development in the Practice*. Heidelberg: Springer.

[6] Augustine, S., Lakshminarasamma, N., and Mishra, M. K. 2016. "Control of Photovoltaic-Based Low-Voltage DC Micro Grid System for Power Sharing with Modified Droop Algorithm." *IET Power Electron.* 9 (6): 1132-43.

[7] Kazmierkowski, M. P., Krishnan, R., and Blaabjerg, F. 2012. *Control in Power Electronics*. Elsevier Science.

[8] Senjyu, T., Miyazato, Y., Yona, A., and Urasaki, N. 2008. "Optimal Distribution Voltage Control and Coordination with Distributed Generation." *IEEE Trans. Power Deliv.* 23: 1236-42.

[9] Ibrahim, H. E. A., and Ibrahim, M. 2012. "Comparison Between Fuzzy and P&O Control for MPPT for

Photovoltaic System Using Boost Converter." *Journal of Energy Technologies and Policy* 2 (6).

[10] Amirnaser, Y., and Reza, I. 2010. *Voltage-Sourced Converters in Power Systems.* Wiley-IEEE Press. ISBN: 978-0-470-52156-4.

[11] Bui, V. H., Chan, T. M., and Nguyen, V. L. 2014. "Controlling AC Power through Multi-step AC-DC-AC-AC Converter with High Frequency Intermediate Stage." *Technical Journal of Control and Automation, December*. (in Vietnamese)